Engineering Structures 56 (2013) 1848–1857

Contents lists available at SciVerse ScienceDirect

Engineering Structures

journal homepage: www.elsevier.com/locate/engstruct

Subassembly testing and modeling of self-centering steel plate shear walls

Patricia M. Clayton *, Jeffrey W. Berman, Laura N. Lowes

Department of Civil and Environmental Engineering, University of Washington, Box 352700, Seattle, WA 98195, USA

ARTICLE INFO

Article history:
Received 11 April 2013
Revised 18 June 2013
Accepted 20 June 2013
Available online 12 September 2013

Keywords:
Self-centering
Post-tensioned connection
Steel plate
Shear wall
Experimentation
Numerical model

ABSTRACT

Experimental and numerical studies have shown self-centering steel plate shear walls (SC-SPSWs) to exhibit enhanced performance including recentering during extreme loading, making them a viable lateral load resisting system for high seismic regions capable of reducing structural repair costs and loss of building functionality after an earthquake. SC-SPSWs utilize thin steel web plates to provide lateral load resistance and energy dissipation, while rocking post-tensioned (PT) beam-to-column connections recenter the building and, if properly designed, eliminate costly damage to the boundary frame. A series of quasi-static cyclic tests have been conducted on SC-SPSW subassemblages. The purpose of these tests is to better understand SC-SPSW and component behavior and the impact of certain web plate and PT connection parameters on performance. This paper presents the results from the test program and also compares the experimental results to those of simple numerical models.

1. Introduction

The self-centering steel plate shear wall (SC-SPSW) has been developed as a resilient lateral load resisting system leveraging the strength and energy dissipating qualities of unstiffened steel web plates and the recentering capabilities of a post-tensioned (PT) boundary frame [1,2]. The beams, also referred to as horizontal boundary elements (HBEs), are connected to the columns, similarly known as vertical boundary elements (VBEs), via PT strands running along the length of the beams. Lateral load is primarily resisted via development of a diagonal tension field in the web plates (as shown in Fig. 1). During lateral sway, the PT beam-to-column connections rock about the beam flanges, the initiation of which is referred to as connection decompression, causing the PT elements to elongate, thus producing the restoring forces necessary to recenter the building [3]. As the PT boundary frame remains elastic to provide recentering, the web plates act as replaceable energy dissipating fuses, distributing yielding up the height of the wall.

Performance-based and capacity design procedures have been developed to ensure adequate seismic performance of the SC-SPSW system and its components [1,2]. Numerical studies have been conducted on a series of SC-SPSWs to verify that the proposed design procedures are capable of achieving the intended performance objectives at different seismic hazard levels in a region of high seismicity [1]. Experimental studies using SC-SPSW subassemblages were also conducted to gain a better understanding of behavior and to experimentally verify response and component demand parameters that are used in design.

The first phase, Phase I, of subassemblage testing [4] investigated how variations in design parameters such as web plate thickness, t_w, number of PT strands, N_s, and initial PT force, T_o affected system, PT strand, and PT connection responses. The results of these tests showed that the experimental behavior qualitatively compared well with the assumed idealized behavior. One key difference, however, was that the actual web plate appeared to provide some compressive resistance during unloading that is commonly assumed to be negligible [5]. This compressive resistance is believed to be due to geometric stiffening of the inelastically buckled web plate during unloading and reformation of the tension field in the opposite loading direction. As the web plate unloading resistance, referred to as web plate residual strength, is proportional to web plate thickness, specimens with thicker web plates were shown to have larger residual drifts at zero-force during cyclic loading at increasing drift demands. Although the SC-SPSW specimens were able to recenter, the web plate residual strength was thought to negatively impact SC-SPSW recentering capabilities based on these quasi-static test results.

A second phase, Phase II, of subassemblage testing was conducted to investigate additional SC-SPSW design variations including HBE depth, web plate-to-fish plate connection detailing, and

* Corresponding author. Tel.: +1 9196108151.
E-mail addresses: clayp@uw.edu (P.M. Clayton), jwberman@uw.edu (J.W. Berman), lowes@uw.edu (L.N. Lowes).

0141-0296/$ - see front matter © 2013 Published by Elsevier Ltd.
http://dx.doi.org/10.1016/j.engstruct.2013.06.030

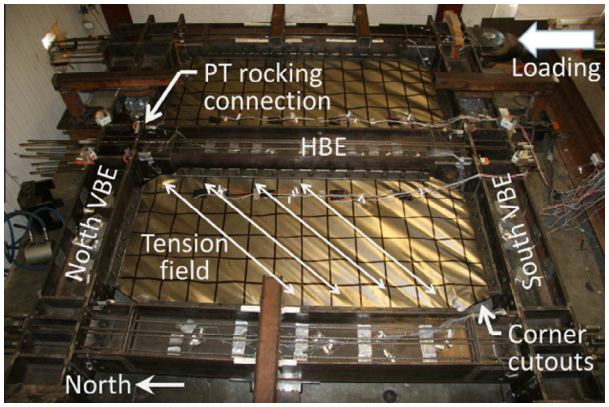

Fig. 1. Typical specimen in deformed configuration (shown at 2% drift).

web plate-to-boundary frame connectivity. This paper presents the results of this phase of testing and a comparison with results of simple numerical analyses. The observations and modeling techniques presented may be used as tools to better inform SC-SPSW design.

2. Description of subassembly tests

The experimental subassembly, as shown in the deformed configuration in Fig. 1, was designed to simulate the boundary conditions of a HBE mid-height in a SC-SPSW, resulting in a two-story configuration with PT beam-to-column connections at all three HBEs. The actuator loaded the specimens at the top of the South VBE. The VBE boundary conditions were simulated with a pinned base under the South VBE and a horizontal roller under the North VBE to allow frame expansion resulting from the rocking behavior of the PT connections [3]. As the intent of these subassembly tests were to characterize SC-SPSW and component behavior, complexities of building applications such as gravity loads, column-to-foundation fixities, and diaphragm-to-SC-SPSW interfaces were not considered. The specimen frame dimensions were 3235 mm from VBE centerline-to-centerline, 1724 mm from HBE centerline-to-centerline, and 4178 mm from center of pin-to-actuator. Drawings of the test setup and PT connection details can be found in Clayton et al. [4].

Table 1 gives a description of all of the SC-SPSW subassembly tests including those from the Phase I of testing [4], as indicated by an asterisks (a). The specimen naming convention was HBE depth (e.g. "W18"), followed by number of PT strands per HBE (e.g. "8s"), initial PT force per HBE in units of kips (e.g. "100k"), web plate gage thickness (e.g. "20Ga"), and any additional descriptors as necessary. The following specimen design parameters are provided in Table 1: web plate thickness, t_w; web plate yield strength, $\sigma_{y,w}$; number of PT strands per HBE, N_s; initial PT force per beam, T_o; and beam depth including any flange reinforcing plates at the connections, d. Phase II of testing most notably investigated the effects of the following parameters: displacement history (W18-8s100k20Ga-2), different web plate thicknesses above and below the middle HBE (W18-8s100k16Ga20Ga), web plate-to-fish plate connection details (W18-8s100k20GaW) and configurations (W14-8s100k16GaHBE), and beam depth.

The load protocol used in Phase II (LP2) had slightly fewer cycles at low drift amplitudes than that of Phase I (LP1), which was based on the displacement history presented in ATC-24 [6,7]. LP2 comprised two cycles at target peak drifts of 0.08%, 0.1%, 0.25%, 0.5%, 1%, 1.5%, 2%, 2.5%, 3%, 4%, 4.5%, and up to 5% when possible [8]. Due to their bilinear ealstic response, PT boundary frame specimens (i.e. those without web plates) were loaded with an abbreivated load history (BF) as described in Clayton et al. [4].

The boundary frame members were designed to remain fully elastic throughout the entire test program and were all of ASTM A992 steel. The VBEs were W14 × 132 shapes and the HBEs were either all W18 × 106 or W14 × 90 shapes depending on the specimen as indicated in Table 1. The PT strands were all 13 mm diameter Grade 270 strands that were placed symmetrically on either side of the HBE webs and were anchored with single strand barrel anchors at the VBE flanges. The web plates were all ASTM A1008 steel. The bolted and welded web plate-to-fish plate connection details are shown in Fig. 2.

The construction sequence of the specimen began with assembling the boundary frame. Each PT strand was stressed individually to the desired initial PT force, as measured by a load cell along each strand. In the laboratory, the initial PT force was adjusted with a threaded spacer, essentially acting as a continuously adjustable shim. In practice, the PT strands could be stressed using a calibrated hydraulic ram to achieve the target PT force. After the PT strands were stressed, the web plates were installed using either the bolted or welded connection detail. Lateral bracing (visible in Fig. 1) was provided along the bottom and top HBEs and

Table 1
SC-SPSW subassembly specimen descriptions.

Specimen name	t_w (mm)	$\sigma_{y,w}$ (MPa)	N_s	T_o (kN)	d (mm)	Loading	Web plate conn.
W18-8s100k[a]	–	–	8	445	526	BF	–
W18-8s100k20Ga[a]	0.92	186	8	445	526	LP1	Bolted
W18-6s75k20Ga[a]	0.92	179	6	334	526	LP1	Bolted
W18-6s75k16Ga[a]	1.52	224	6	334	526	LP1	Bolted
W18-8s100k16Ga[a]	1.52	238	8	445	526	LP1	Bolted
W18-6s75k	–	–	6	334	526	BF	–
W18-8s100k20Ga-2	0.92	196	8	445	526	LP2	Bolted
W18-8s100k16Ga20Ga	1.52(1st)	251	8	445	526	LP2	Bolted
	0.92(2nd)	184					
W18-8s100k20GaW	0.92	204	8	445	526	LP2	Welded
W14-6s75k	–	–	6	334	381	BF	–
W14-8s100k16Ga	1.52	180	6	334	381	LP2	Bolted
W14-8s100k16GaHBE	1.52	208	6	334	381	LP2	Bolted (HBEs only)
W14-8s100k20Ga	0.92	177	8	445	381	LP2	Bolted
W14-6s75k20Ga	0.92	165	6	334	381	LP2	Bolted

[a] Tests conducted in Phase I and presented in [4].

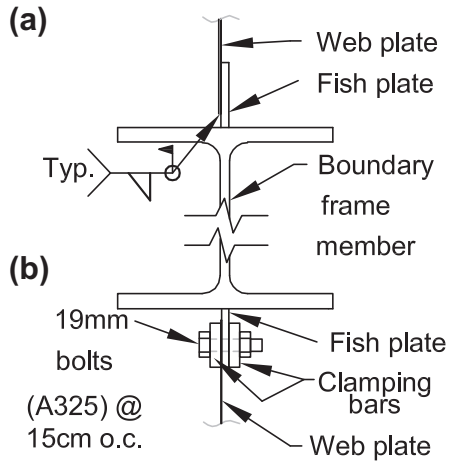

Fig. 2. (a) Welded and (b) bolted web plate-to-fish plate connection details.

along the VBEs to prevent displacement of the frame in both out-of-plane directions. Lubricated stainless steel and polytetrafluoroethylene (PTFE) interfaces were provided to reduce friction forces between the specimen and the lateral bracing. The PT strands were destressed and restressed between each specimen.

The specimens were instrumented with displacement potentiometers to measure global column displacements and PT connection gap opening. Strain gages were also installed along the HBEs and VBEs to measure the strain profile at certain points [8]. This data was used to estimate the moment and axial force demands in the components by assuming elastic cross-sectional properties and that plane sections remain plane. Uniaxial and rosette strain gages were also placed on the web plates in some specimens to measure local strains at the web plate corner cutouts near the PT connections and principal strains in the tension field [8].

3. Experimental results and observations

Experimental results and observations are described below as they relate to variations in certain test parameters investigated in Phase II of testing. For comparison, Table 2 provides several performance parameters including the drift at which certain damage states are first observed, the peak strength and associated drift, and the specimen strength (normalized by the peak strength) and maximum drift during the last cycle of loading. The key damage states documented here include first observance of web plate tearing, $DS_{tear,i}$ (corresponding to DS9 in Baldvins et al. [9]) and first observance of a tear propagating along an entire HBE or VBE edge, $DS_{tear,u}$. Note that in none of the tests was any boundary frame or PT yielding observed. Also note that the test of W18-8s100k16Ga was terminated prior to the observance of web plate tearing due to PT wire fracture. The wire fracture was due to reuse of the PT strands for numerous tests as described in Clayton et al. [4] and is not believed to be of concern in actual SC-SPSW applications.

3.1. Effects of load protocol

Specimens W18-8s100k20Ga and W18-8s100k20Ga-2 were essentially the same but were loaded with different displacement histories, LP1 and LP2, respectively. The differences in the displacement histories were subtle—the main difference being LP2 had eight fewer cycles at small drift amplitudes, less than 2%, than LP1. The target displacements above 1.5% drift in LP2 were based on quasi-static tests of conventional SPSWs [7,10].

Both of these specimens showed initial signs of web plate tearing at drifts slightly less than 3% (Table 2) and both lost approximately 13% of their peak strength during the second cycles of loading at 3.7% and 3.8% drift for specimens W18-8s100k20Ga and W18-8s100k20Ga-2, respectively. These observations of web plate tearing and strength degradation suggest that web plate damage is not significantly affected by number of cycles at low displacement amplitudes, at least for the the specimens and web plate connection detailing considered here; therefore, the remainder of the tests were conducted using LP2 for simplicity.

3.2. Effects of beam depth

As shown in Clayton et al. [4], the SC-SPSW recentering stiffness, K_r, is directly proportional to the post-decompression PT connection rotational stiffness, k_d^θ:

$$k_d^\theta = \frac{d^2}{2}\left(\frac{k_{PT}k_{HBE}}{k_{PT}+k_{HBE}}\right) \quad (1)$$

where d is the depth of the HBE at the connection and k_{PT} and k_{HBE} are the axial stiffnesses of all the PT strands and the HBE at a particular level, respectively. In the case of these specimens, where k_{HBE} is significantly larger than k_{PT}, the PT connection rotational stiffness, k_d^θ, is related primarily to d^2 and k_{PT}. Fig. 3 compares the force vs. drift response of two specimens that are essentially identical with the exception of HBE depth. The recentering stiffness, K_r, of each specimen was determined from linear regressions of the unloading portions of the experimental specimen response as shown in Fig. 3. The recentering stiffness of specimens W14-8s100k20Ga and W18-8s200k20Ga-2 were found to be 0.97 and 1.87 kN/mm, respectively,

Table 2
Subassembly test damage observations.

Specimen name	Drift (%)		V_{max} (kN)	Drift at V_{max} (%)	V_{end}/V_{max}	Max. Drift (%)
	$DS_{tear,i}$	$DS_{tear,u}$				
W18-8s100k20Ga	2.8	3.6	810	2.8	0.81	3.7[a]
W18-6s75k20Ga	2.6	–	706	3.1	0.87	4.2
W18-6s75k16Ga	3.6	4.2	1102	3.7	0.73	4.7
W18-8s100k16Ga[b]	–[b]	–[a]	1064[b]	2.5[b]	1.0[b]	2.5[b]
W18-8s100k20Ga-2	2.9	4.4	833	3.8	0.81	4.4
W18-8s100k16Ga20Ga	2.4	–	1004	4.5	0.95	5.0
W18-8s100k20GaW	0.7	4.0	706	3.9	0.91	5.0
W14-8s100k16Ga	3.0	4.5	800	3.9	0.86	4.5
W14-8s100k16GaHBE	4.5	–	586	4.5	0.87	5.0
W14-8s100k20Ga	3.0	4.0	576	3.7	0.62	5.0
W14-6s75k20Ga	3.0	4.5	504	3.8	0.63	4.5

[a] Target drift was 4.5%. Actual drifts were less than target drifts due to controller scaling, which was corrected in later tests.
[b] Test was ended prematurely due to PT wire fracture [4].

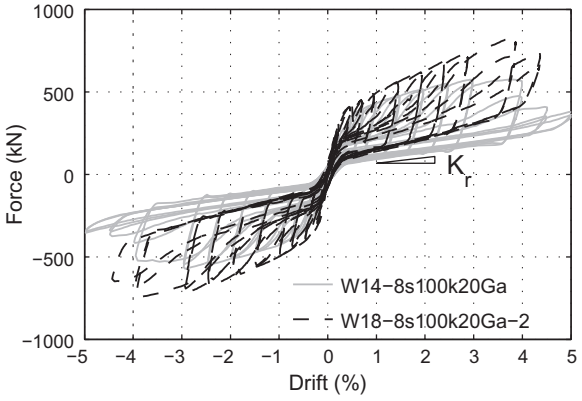

Fig. 3. Comparison of specimens with different beam depth.

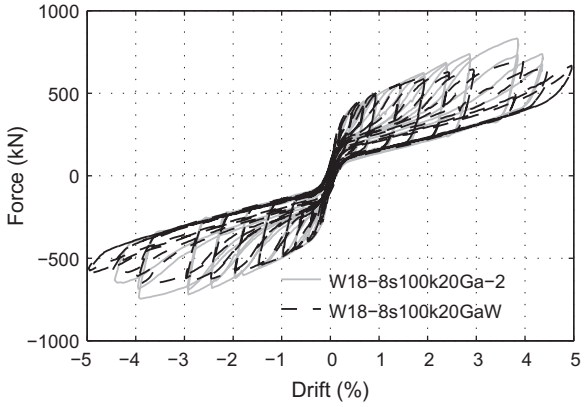

Fig. 5. Comparison of specimens with bolted (W18-8s100k20Ga-2) and welded (W18-8s100k20GaW) web plate-to-fish plate connection details.

resulting in a ratio, $K_{r,W14}/K_{r,W18}$, of 0.521. As both specimens had the same number of PT strands, this value is roughly equal to the ratio d^2_{W14}/d^2_{W18} of 0.525, verifying the expected relationship between HBE depth and recentering stiffness.

The effect of HBE depth on PT connection rotational stiffness and recentering stiffness is also illustrated in the PT force vs. drift response for the middle HBE (Fig. 4). The PT elongation, and thus PT force, is larger in the W18 specimen than in the W14 specimen for a given drift demand due to the increase in connection rocking depth. As the development of PT strain energy provides the restoring forces to recenter the frame, the lower PT elongation at a given drift demand caused by a decrease in HBE depth results in a lower recentering stiffness and corresponding PT connection rotational stiffness.

3.3. Effects of web plate connection details

Fig. 5 shows the force vs. drift response of specimens with bolted (W18-8s100k20Ga-2) and welded (W18-8s100k20GaW) web plate-to-fish plate connection details (shown schematically in Fig. 2). All other specimen parameters were identical between the two specimens. As observed in Fig. 5 the two specimens have essentially identical response up to 1.5% drift.

Initial signs of web plate tearing were first observed in specimen W18-8s100k20GaW at 0.7% drift with very small cracks, less than 5 mm, at the toe of the weld along the first story VBE (Table 2, Fig. 6a). All web plate tearing initiated at the toe of the weld and propagated just outside of the heat affected zone (HAZ). Tear propagation was minimal up to 2% drift, with tear lengths not exceeding 10% of the total weld length along a given edge.

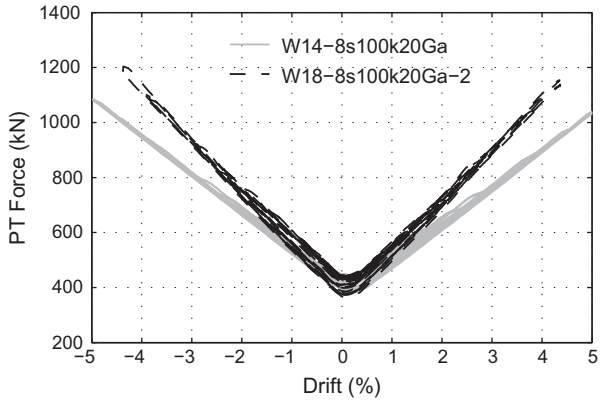

Fig. 4. Comparison of total PT force in middle HBE for specimens with different beam depth.

In a survey of conventional SPSW tests, all of which used welded web plate connection details, initial web plate tearing was first recorded at a median drift of 1.6% [9], which is greater than the observation of tearing at 0.7% drift in this specimen; however, it is not outside of the range of conventional SPSWs as some tests did have web plate tearing at lower drift levels [11,12]. The earlier onset of web plate tearing in SC-SPSWs can be explained by the additional web plate demands resulting from gap opening and out-of-plane web plate deformation along the unrestrained edge of the corner cutouts in SC-SPSWs that are not present in conventional SPSW web plates welded continuously along all edges.

At 2% drift the welded specimen strength was approximately 96% of the bolted specimen, and this ratio decreseased with increasing drift demands. During the second cycle at 4% drift, the first story web plate of W18-8s100k20GaW tore completely through along a VBE edge; however, the specimen retained 91% of its peak strength after two cycles at 5% drift with at least one third of the web plate edge being intact along all of the HBEs.

Tearing was first observed in the specimen with the bolted web plate connection detail (W18-8s100k20Ga-2) at 2.9% drift (Table 2, Fig. 6b); however, minor web plate slip was observed at the ends of the clamping bars as early as 0.75% drift in the 8 cm beyond the outermost bolts where the clamping friction forces were reduced (shown at 2.9% drift in Fig. 6b). Tearing typically initiated and propagated along the edge of the clamping bars. In specimen W18-8s100k20Ga-2, the tear propagated along the entire length of the bottom HBE after two cycles at 4.4% drift, retaining 81% of its peak strength.

While the peak strength of the specimen with the welded web plate connection was 85% of that with the bolted web plate connection, and the welded connection detail showed signs of web plate tearing prior to the bolted connection detail, both specimens had similar strengths up to 2% drift, within the range of design-level earthquake drift demands [1]. Interestingly, both specimens had nearly identical unloading strength and stiffness even though they had significantly different peak strengths and web plate tearing characteristics. This observation indicates that the web plate residual strength does not degrade significantly with web plate peak strength and damage, supporting the hypothesis that web plate residual strength is a product of the geometric stiffness of the buckled and plastically deformed web plate as it deforms during unloading.

3.4. Effect of web plate configuration

Fig. 7 shows the force vs. drift response of specimens with the web plates connected along all edges (W14-8s100k16Ga) and

Fig. 6. Photos of first observations of tearing in specimens (a) W18-8s100k20GaW and (b) W18-8s100k20Ga-2.

along the HBEs only (W14-8s100k16GaHBE). Connecting the web plates only to the HBEs delayed the onset of web plate tearing, which was first observed at 4.5% drift in specimen W14-8s100 k20GaHBE compared to 3% drift in specimen W14-8s100k20Ga (Table 2). Connecting the web plate to the HBEs only similarly increased specimen ductility, with W14-8s100k20GaHBE sustaining two cycles of loading at 5% drift with minimal tearing (less than 33% of the edge length torn along the most damaged edge) while the first story web plate in W14-8s100k20Ga tore completely along the edge of the middle HBE after two cycles at 4.5% drift (Table 2).

The strength of the specimens with web plates connected to the HBEs only is significantly less than the specimen with web plates connected to the boundary frame along all edges due to the decrease in the size of the tension field. The total web plate strength, calculated as the peak strength minus the unloading strength of each specimen at 2% drift, for W14-8s100k20GaHBE was 52% of W14-8s100k20Ga. This is consistent with visual observations of the extent of the diagonal buckles of the tension field. Due to lack of restraint along the vertical edges, a partial tension field develops along just over half of the horizontal edge length and at a steeper angle of inclination [13,14] in W14-8s100k20GaHBE (Fig. 8). This observation can be compared to the tension field developed along the full horizontal edge length and at an approximately 45 degree inclination in specimens with the web plate connected along all edges (e.g. Fig. 1).

By releasing the web plate from the VBEs, the component of axial force in the HBE due to the web plates pulling in the VBEs, termed $P_{HBE,VBE}$ in Sabelli and Bruneau [5], is eliminated. Fig. 10 shows the average axial force, as calculated from strain gage measurements, in the middle HBE during the 2% cycle for the

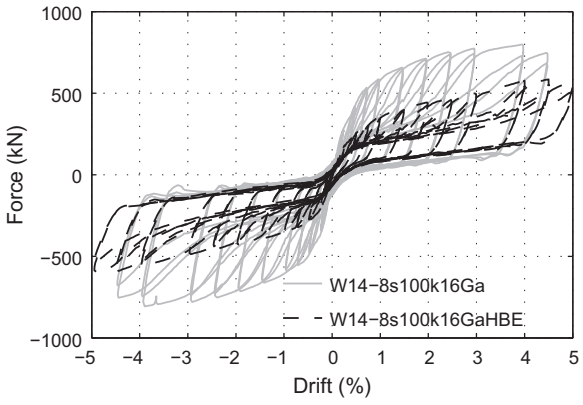

Fig. 7. Comparison of specimens with web plate connected along all edges (W14-8s100k16Ga) and along the HBEs only (W14-8s100k20GaHBE).

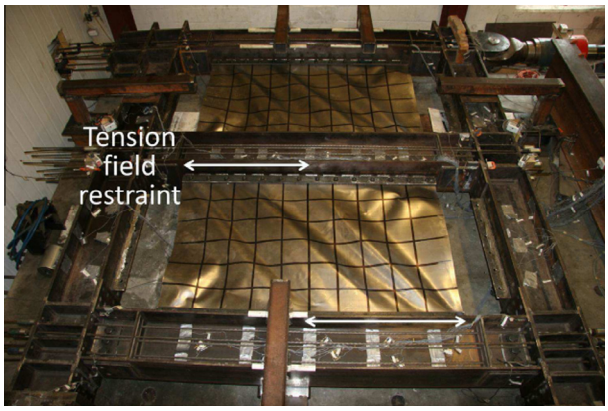

Fig. 8. Specimen W14-8s100k20GaHBE at 2% drift.

specimens with web plates connected along all edges (W14-8s100k20Ga) and along the HBEs only (W14-8s100k20GaHBE). This figure is most effective at demonstrating typical intermediate HBE axial force response and comparing the relative magnitudes of the different components of the HBE axial force. The HBE axial load is influenced primarily by three components [2]: the increase in PT force as the PT connection gap opens; the difference in web plate thicknesses or strengths above and below the HBE, which is not the case for either of these specimens; and the web plate pull-in of the VBEs. The change in PT force is due primarily to the connection gap opening which can be related to drift. As shown in Fig. 9, the PT force increase with respect to drift is not significantly impacted by the web plate-to-boundary frame connectivity. As such, the size of the hysteretic loop in the the average HBE axial force response (Fig. 10) of W14-8s100k20Ga can be attributed to the VBE pull-in. As the web plate stress and corresponding pull-in of the VBEs increases, as does the HBE axial load (as indicated by the increase in magnitude of compressive forces). The quick reduction in web plate force just as the specimen begins unloading results in a rapid decrease in HBE axial load, the magnitude of which corresponds to $P_{HBE,VBE}$. After the initial unloading of the web plate, the HBE compression demands decrease in proportion to the decrease in PT forces. Alternatively, in W14-8s100k20GaHBE, where the VBE pull-in is eliminated, the hysteretic loop is essentially nonexistent. In this specimen, the HBE axial load depends mainly on the PT force.

The significant delay and reduction of web plate tearing in the specimen with the web plate connected to the HBEs only suggests that much of the web plate damage in other specimens can be attributed to the effects of gap opening and frame expansion causing increased horizontal strain demands in the web plate. If the web plate thickness is appropriately designed to resist the required

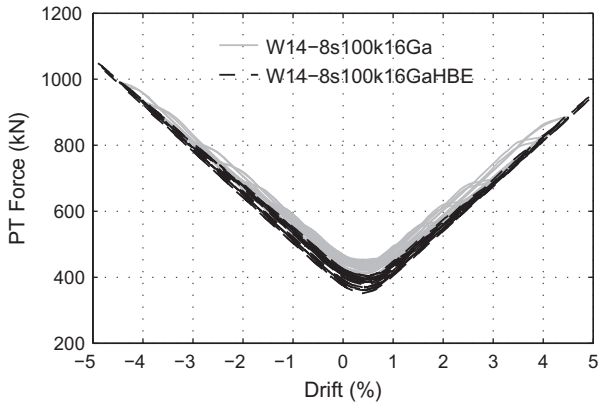

Fig. 9. Comparison of PT force in middle HBE of specimens with web plate connected along all edges (W14-8s100k16Ga) and along the HBEs only (W14-8s100k20GaHBE).

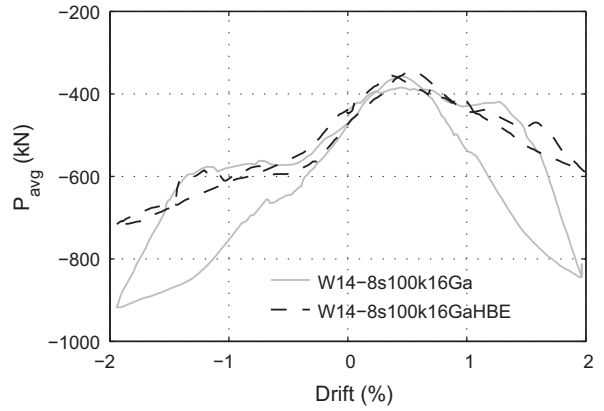

Fig. 10. Comparison of average measured axial force in specimens with web plate connected along all edges (W14-8s100k16Ga) and along the HBEs only (W14-8s100k20GaHBE) during 2% cycle.

lateral loads, using a HBE-only web plate connection configuration may be desirable in SC-SPSWs for web plate damage mitigation and potential reduction of VBE demands [15].

4. Numerical model

4.1. Description of model

The test specimens were modeled in OpenSees [16] as shown schematically in Fig. 11. The boundary frame elements were modeled using force-based beam-column elements with fiber cross-sections to allow for distributed plasticity, although no yielding was expected. The PT elements were modeled using truss elements with an initial stress (using the Steel02 material in OpenSees) and were anchored at points rigidly offset half the column depth outside of the VBE centerline. The boundary frame and PT elements were modeled with the nominal elastic moduli and yield strengths of their respective materials. The web plate was modeled using diagonal strips oriented in both directions of the tension field [5]. The strips in the models with web plates connected to HBEs and VBEs were inclined at an angle, α, of approximately 45° according to the equation in Sabelli and Bruneau [5]. For specimen W14-8s100k16GaHBE, the strips were connected to the HBEs only as shown in Fig. 12. Here, the strip inclination, θ, was calculated to be approximately 30° from vertical as determined from the equation $tan(2\theta) = h/L$ presented in Thorburn et al. [14] for web plates

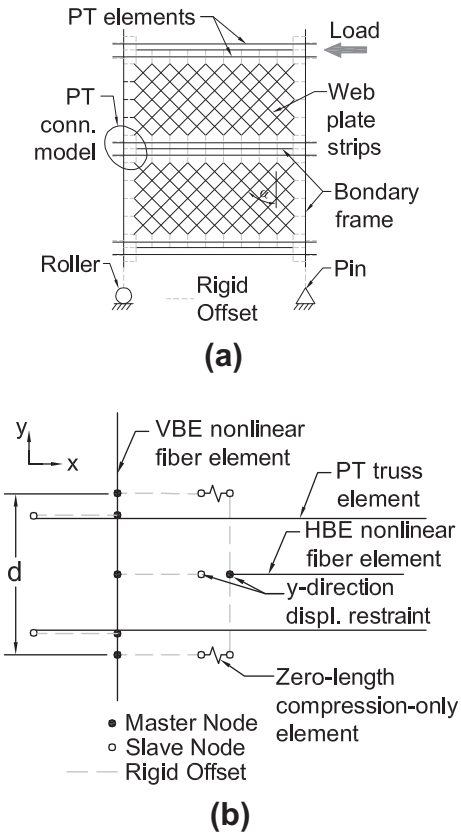

Fig. 11. Schematic of numerical model of (a) specimen and (b) PT connection.

with no vertical boundary restraint, where h and L are the web plate height and length, respectively. All strips were rigidly offset half of the corresponding boundary element depth from the boundary frame centerline. Details of the strip material model will be discussed later. The pin and roller boundary conditions at the base of the VBEs corresponded to those in the physical experimental model.

The PT connection (Fig. 11b) was modeled using compression-only zero-length elements rigidly offset from the boundary elements to simulate gap opening and closing at the HBE flanges. Shear forces were transferred from the HBEs to VBEs in the model via vertical displacement restraints (using the equalDOF command in OpenSees) between the VBE flange and HBE centerline simulating the horizontally slotted shear tab connection in the physical model. The vertical restraint used here has a similar effect to the diagonal shear transfer springs used in Clayton et al. [1], producing nearly identical system and connection responses.

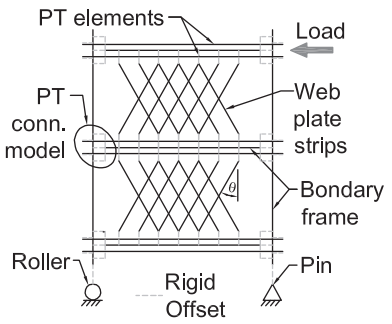

Fig. 12. Schematic of numerical model of specimen with web plate connected to HBEs only.

Sabelli and Bruneau [5] suggest modeling the web plate using tension-only strips with a pinched hysteresis under the assumption that web plate shear buckling strength is negligible resulting in immediate formation of the tension field, that web plates have negligible stiffness upon unloading, and that the web plate must reach the previous peak plastic strain before resisting additional load. This idealized tension-only web plate behavior (shown as Model TO in Fig. 13) has been shown to match the initial stiffness, strength, and cyclic response in conventional SPSWs [5] with moment-resisting HBE-to-VBE connections reasonably well.

In Phase I of SC-SPSW testing presented in Clayton et al. [4], the specimens were observed to have additional energy dissipation upon unloading that was attributed to the web plate residual strength, $V_{web,resid}$. This web plate residual strength was also observed in conventional SPSW experiments [17] when assumed boundary frame response was removed from the specimen response to approximate the web plate contribution; however, the impact and magnitude of $V_{web,resid}$ was overshadowed by the significant supplementary strength and energy dissipation provided by the moment-resisting boundary frame.

In SC-SPSWs, where the PT boundary frame offers no energy dissipative qualities and where unloading strengths of the web plates can have an impact on recentering capabilities, proper modeling of $V_{web,resid}$ is necessary. Previous research [18] proposed a modified strip model to account for the additional resistance of the "compressive field" in the web plate by including a compression-only diagonal strut with a strength of 8% of the web plate tension yield strength; however, this compressive strength was lower than those estimated from previous SC-SPSW testing [4]. To simulate this residual strength phenomenon, a modified strip material was used in which a pinched tension-only material, as described above, and an elastic-perfectly plastic compression-only material are used in parallel. Here, the compression-only material had a compressive strength equivalent to 25% of the web plate tensile yield strength. Since the residual web plate strength phenomenon only affects lateral strength during web plate unloading and reformation of the tension field, the strip tensile strength must be reduced by the same 25% such that the peak lateral load resistance of the web plate modeled with strips oriented in both tension field directions is the same as the the tension-only strip model. This reduction in strip tensile strength is not associated with an actual web plate mechanism; it is numerically simulated to account for the additional lateral load resistance provided by the compressive strength of the strips oriented in the opposite direction of the tension field. The cyclic response of the tension-only strip material (Model TO) and the modified tension–compression strip material (Model TC) with compressive strength equal to 25% of the plate material tension yield strength is shown in Fig. 13. The yield envelope for each web plate was fit to monotonic tensile tests of coupons taken from each plate, shown for one particular coupon in Fig. 13.

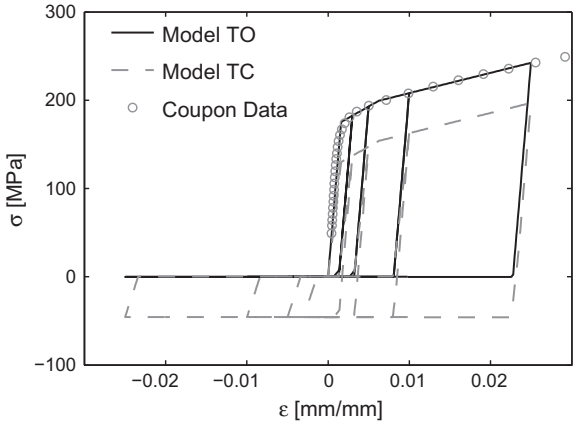

Fig. 13. Web plate tension-only ('Model TO') and tension–compression ('Model TC') strip material models fit to monotonic coupon test data.

4.2. Comparison of response

Fig. 14 shows a comparison of the experimental and numerical model force vs. drift responses for specimen W14-8s100k20Ga and is representative of typical subassembly specimens. Fig. 14a shows the numerical results from the model with the tension-only strips, while Fig. 14b shows the numerical results for the modified tension–compression strip model with compressive strength equal to 25% of the web plate yield strength. For clarity, the numerical models shown here were subjected to cycles at 1.5% and 2% drift only to show characteristics of the response envelope and the unloading and reloading behavior for a cycle prior to web plate tearing. The 2% drift cycles are shown in solid lines for better comparison of a single cycle response.

Both numerical models overestimate the initial stiffness, which is likely due to the numerical assumption that the PT connections have a stiffness equivalent to a welded connection prior to decompression [4,3]; however, the actual connections have uneven bearing surfaces at the HBE flanges due to construction tolerances, allowing for some connection rotation prior to reaching the decompression moment, M_d. The models both have similar yield envelopes, both of which seem to accurately approximate initial

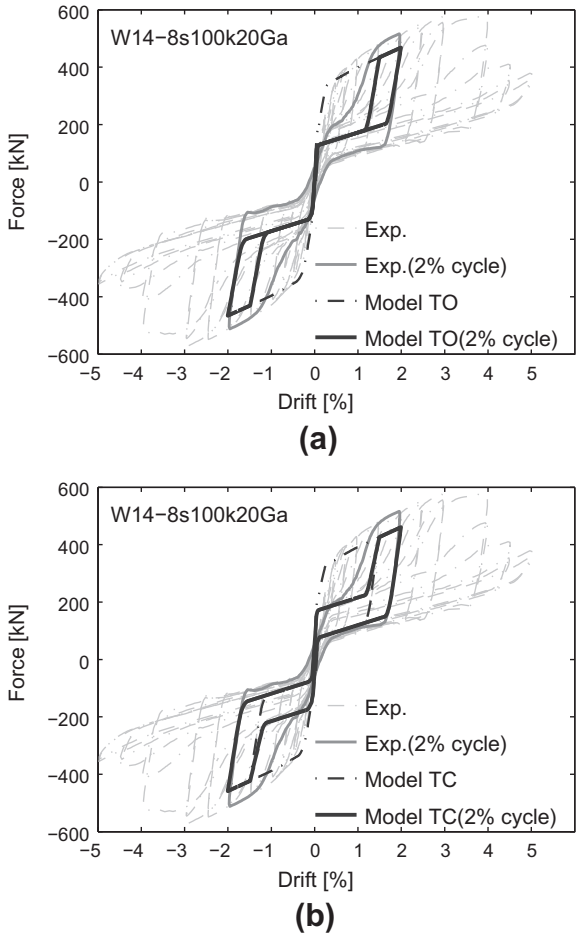

Fig. 14. Comparison of specimen W14-8s100k20Ga response with (a) tension-only ('Model TO') and (b) tension–compression ('Model TC') strip model responses.

web plate yielding but underestimate strain hardening in the yield surface.

The underestimation of strain hardening is believed to be due to the continuum nature of the web plate not simulated in the strip model—as the web plate yields in the tension field direction, the direction perpendicular to the tension field is contracting due to the Poisson effect. This contraction causes the plate to yield and accumulate plastic strain in the direction perpendicular to the tension field [19], which increases the rate of strain hardening compared to the traditional strip model. Based on the experimental drift history, the accumulated plastic strain can be up to four times that which is assumed by the strip model [19]. Depending on the web plate material stress-strain response, this increase in plastic strain accumulation can result in tensile stresses typically around 20–30% higher than the stress assumed in a traditional strip model. This difference corresponds to the magnitude by which the strip model underestimates the web plate strength as shown in Fig. 14. The strip model underestimation of web plate strength was typical in specimens with bolted web plate-to-fish plate connections in which tearing was initiated after 2% drift. In the specimen with welded web plate connections where tearing was observed prior to reaching 2% drift, the strip model overestimation is not apparent. Although the current strip modeling methods are conservative in predicting web plate srength, further research should be done to quantify the amount of plastic strain accumulation in the web plate continuum. Future improvements to the strip model should account for this increased rate in strain hardening.

The stiffness of the unloading portions (i.e. K_r) of the numerical responses match well with the experimental response; however, by intent, both models have different strengths at unloading (and subsequent reloading in the next cycle) due to the compressive component of the material model. The unloading and subsequent reloading of the tension-only model (Model TO) follow the same path; however, the tension–compression model (Model TC) unloading path is lower than that of the tension-only, while its reloading path is higher, resulting in additional energy dissipation in the tension–compression model which is also observed in the experimental response. The tension–compression unloading strength is similar to the experimental specimen, accurately estimating the effect of the web plate residual strength. Similarly, the reloading strength of the tension–compression model is similar to the load at which the specimen web plate begins deforming with a lower stiffness; however, the actual web plate does appear to resist additional load earlier in the reloading cycle resulting in greater energy dissipation than the modified numerical model.

While work can still be done to more accurately model the additional energy dissipation in the web plate, the tension–compression model appears to better estimate unloading strengths than the previously assumed tension-only model for the tests shown here. Accurately estimating web plate unloading strengths are important in SC-SPSWs where web plate residual strengths can result in larger residual drifts at zero-force and may decrease recentering robustness. Furthermore, the 25% compressive strength assumed here was an approximation based on Webster [19] which correlates web plate aspect and slenderness ratios to residual strength. Further work should be done to better quantify the web plate residual strength magnitude for a broad range of web plate and load history parameters.

The experimental response in Fig. 14 also shows that the reloading strength of the specimen decreases as the extent of web plate tearing increases at large drifts. At the 5% drift cycles where the web plate was torn completely along the VBEs and along the majority of the HBEs, the reloading strength approaches that of the tension-only model (Fig. 14a). Due to the considerable web plate tearing along the boundary elements, the tension field cannot developed during reloading, which is representative of the tension-only strips that cannot resist additional load until reaching the peak plastic strain from previous cycles. However, in these cycles after significant tearing the specimen unloads with a lower strength, closer to the unloading curve of the tension–compression model. This behavior indicates that although the tension field cannot develop to resist lateral load during reloading, the severely damaged web plate still provides some resistance, and thus energy dissipation upon unloading. This unloading resistance is attributed to the work required to return the hardened, deformed web plate to zero-displacement, indicating that web plate resdiual strength is related to the full web plate stiffness and not the development of the tension field.

Fig. 15 shows a comparison between the experimental and numerical response for W14-8s100k16GaHBE, where the web plate is connected only to the HBEs, with tension–compression strips. Again, the strip model underestimates the strain hardening in the specimen for reasons previously described, and the tension–compression strip model is able to approximate the reloading strength of the web plate. However, one key difference is that the unloading strength of the tension–compression strip model is greater than that of the specimen, meaning that the web plate residual strength is underestimated in the tension–compression partial tension field numerical model. This observation is consistent with the theory that the web plate residual strength is a function of the entire web plate geometric stiffness as described previously. The tension–compression strip model (Fig. 12), which only models the portion of the web plate contributing to the tension field, is able to accurately capture the peak and reloading strengths that depend on tension field action. However, the tension–compression strip model underestimates the web plate residual strength, because it does not account for the additional unloading resistance provided by the portions of the web plate not included in the partial tension field model. Although further work can be done to better understand the behavior of web plates connected only to the HBEs, this simple modeling approach appears to adequately predict web plate strength, and the discrepancies in numerical and experimental responses are consistent with phenomenological theories previously presented.

4.3. Comparison of HBE demands

Dowden et al. [2] provides formulas for determining the HBE axial force and moment demands for design of this critical SC-SPSW component. Fig. 16 compares the moment distribution derived from these formulas, the numerical model, and from experimental strain gage data (shown here for specimens

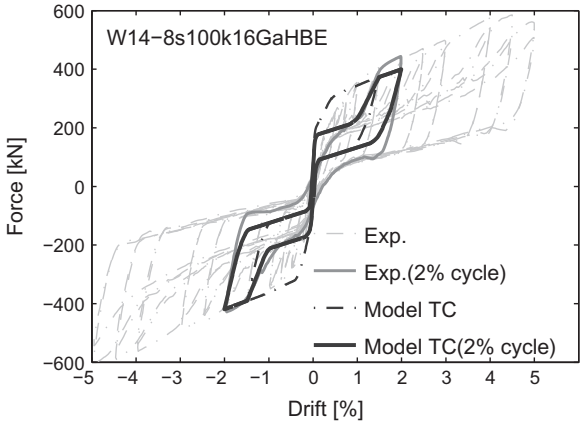

Fig. 15. Comparison of specimen W14-8s100k16GaHBE response and numerical model with tension–compression ('Model TC') strips.

W18-8s100k20Ga-2 and W14-8s100k20Ga at 2% dirft). The experimentally determined moments are derived using the curvature as calculated from a linear regression of the strain gage data at a given location along the HBE length, the elastic modulus of steel (200 GPa), and nominal cross-sectional moments of inertia of the beam. The moments calculated per Dowden et al. [2] assumed a constant web plate stress distribution based on the web plate tension yield strength oriented at an angle, α, of 45°. The calculated moment distribution matches well with the OpenSees numerical model. When the 25% compressive strength is included in the numerical strip material model, the magnitude of the peak moments reduces by approximatly 5% compared to the tension-only strip model.

The linear shape of the moment distribution in Fig. 16 is due to fact that the web plate distributed force above and below the middle HBE are roughly the same. In the case where web plate thicknesses and story shears above and below an HBE are unequal, the moment distribution will have a parabolic shape as illustrated in Dowden et al. [2]. Some variation between the assumed, simulated, and experimental HBE moment distributions may be due to differences in the assumed and actual tension field inclination and stress distribution, web plate strain hardening and PT losses, difference in axial load during positive and negative excursions due to actuator loading on one column, and inherent uncertainty in deriving moments from very small strain measurements. In general, the experimental moments calculated from strain gages followed similar trends and had similar magnitudes as the numerical and analytical approximations, demonstrating that the design formulas and modeling methods presented previously in Dowden et al. [2] and Clayton et al. [1] adequately predict the HBE demands.

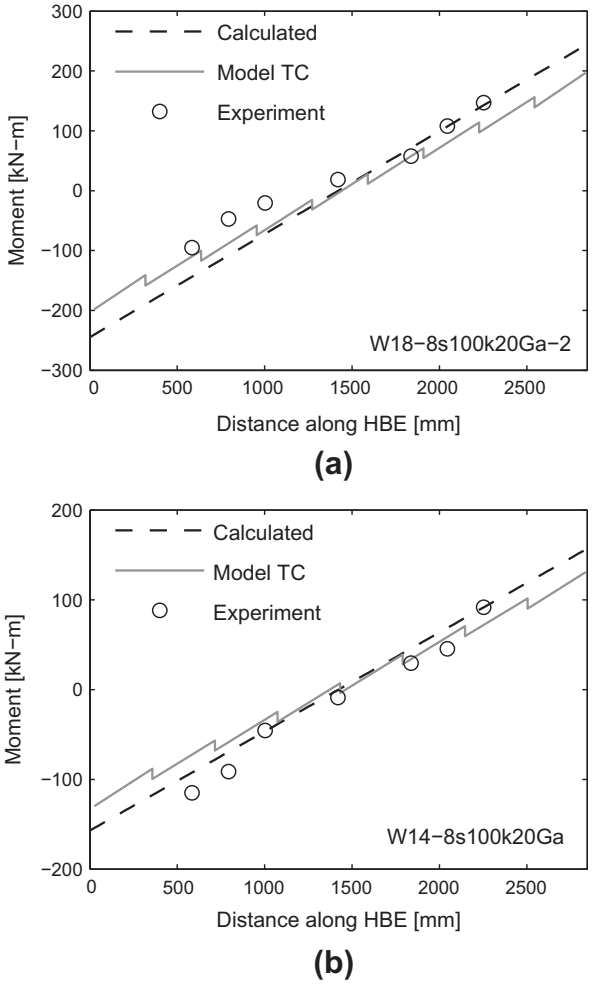

Fig. 16. Moment distribution at 2% drift for specimens (a) W18-8s100k20Ga-2 and (b) W14-8s100k20Ga.

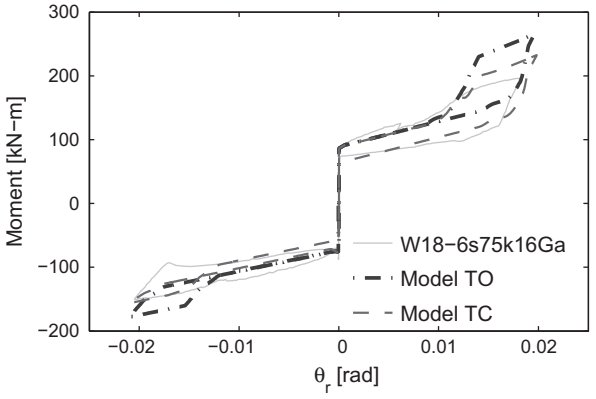

Fig. 17. Comparison of experimental and numerical PT connection response during 2% cycle.

The PT connection response is typically characterized by the HBE moment at the connection vs. relative rotation in the decompressed connection, θ_r. Although the moment at the connection is not measured directly in the experiment, it can be estimated using some simplifying assumptions. If the web plate stress distribution along the HBE is assumed to be constant, if the web plates above and below the HBE have similar thicknesses and yield strengths, as is the case for all specimens but W18-8s100k16Ga20Ga, and if the HBE is assumed to rock about the outside edge of its flanges, then the moment at the connections can be estimated as the average axial force calculated from strain gage data times half the beam depth, $d/2$ [2]. The connection rotation is calculated directly from displacement potentiometers located on each flange at the ends of the HBE. In Fig. 17, an example of the experimentally estimated connection response is compared to the numerical connection responses for W18-6s75k16Ga at the south end of the middle HBE during the 2% cycle. Although it is only an approximation, the experimentally derived response matches well with relative magnitudes and hysteretic trends of the numerical connection response.

5. Conclusions

Quasi-static cyclic testing of SC-SPSW subassemblies have been conducted to understand the impact of design parameters on system behavior and to investigate the demands on an intermediate HBE in a SC-SPSW. Phase I [4] and Phase II of testing considered such design parameters as web plate thickness, t_w, number of PT strands, N_s, initial PT force, T_o, beam depth, d, bolted and welded web plate connection details, and web plate-boundary frame connection configuration. The experimental results were also compared to idealized analytical response and simple SC-SPSW numerical models.

The tests showed that the web plate thickness, t_w, had a significant impact on SC-SPSW strength and energy dissipation as expected, and also had a minor impact on residual drift at zero-force [4], which was attributed to the residual web plate strength caused by geometric stiffening of the plastically deformed web plate during unloading. The number of PT strands, N_s, and beam depth, d, impacted the PT connection rotational stiffness and recentering stiffness, K_r, a key parameter in SC-SPSW design [1].

The bolted web plate connection detail was adequate to transfer web plate forces to the boundary frame with initial observations of web plate tearing typically occurring between 2.5% and 3% drift and complete tearthrough of the web plate typically occuring between 4% and 4.5% drift. Tearing was first observed in the specimen with the welded web plate connection detail at 0.75% drift; however, peak strengths were not significantly different from similar bolted web plate specimens within the range of design-level drift demands up to 2% drift. Tearing along the welded web plate connection was ductile without significant deterioration of strength in loading cycles up to 5% drift.

Connecting the web plates to the HBEs only was also investigated as a means of mitigating web plate damage. This web plate-boundary frame connection configuration greatly delayed the initiation of and reduced the overall extent of web plate tearing by eliminating the localized strains in the corner cutouts and horizontal strains in the web plate associated with PT connection gap opening and frame expansion. However, if implemented in this configuration, the web plate thickness must be properly designed for the strength provided by the partial tension field developed in the web plate without vertical boundary restraints [14].

The test results were compared to a simple numerical model employing nonlinear springs in the PT connections to simulate the rocking behavior and a diagonal strip model to simulate the web plate. The strips were modeled with two strip materials: a tension-only material, as suggested by Sabelli and Bruneau [5] among others, and a tension–compression material, based on a simple modification of the tension strip to include compressive resistance to account for the residual web plate strength described above. The numerical models were able to adequately predicted the specimen response, including yield strength, recentering stiffness, K_r, and HBE moment demands. The tension–compression strip was better at predicting the reloading and unloading strengths of the SC-SPSW specimens than the tension-only model; however, further research can be done to more accurately simulate the complex web plate behavior. Recommended future model improvements include accounting for the increased accumulation of plastic strain in the web plate due to plastic contraction during reverse cyclic loading that is not considered in the strip method, adjusting the strip reloading stiffness to account for the additional strength and energy dissipation during web plate reloading, and better quantifying the amount of web plate residual strength for a broad range of web plate geometric parameters and load histories.

Overall, these tests showed that a properly designed SC-SPSW is capable of recentering when subjected to large drift demands with ductile energy dissipation and yielding occurring in the replaceable web plate elements. Simple analytical and numerical models presented here and in Clayton et al. [4] and Dowden et al. [2] are able to accurately predict key response and demand parameters of SC-SPSW systems and components when compared to experimental results. The experimental results, observations, and numerical models have been presented as tools to better inform design, implementation, and future research directions of the SC-SPSW system.

Acknowledgments

Financial support for this study was provided by the National Science Foundation as part of the George E. Brown Network for Earthquake Engineering Simulation under Award Number CMMI-0830294. P. Clayton was also supported by the National Science Foundation Graduate Research Fellowship under Grant No. DGE-0718124. The authors would also like to acknowledge material donations from the American Institute of Steel Construction. Any opinions, findings, conclusions, and recommendations presented in this paper are those of the authors and do not necessarily reflect the views of the sponsors.

References

[1] Clayton PM, Berman JW, Lowes LN. Seismic design and performance of self-centering steel plate shear walls. J Struct Eng 2012;138:22–30.
[2] Dowden DM, Purba R, Bruneau M. Behavior of self-centering steel plate shear walls and design considerations. J Struct Eng 2012;138:11–21.
[3] Garlock MM, Sause R, Ricles JM. Behavior and design of posttensioned steel frame systems. J Struct Eng 2007;133(3):389–99.
[4] Clayton PM, Winkely TB, Berman JW, Lowes LN. Experimental investigation of self-centering steel plate shear walls. J Struct Eng 2012;138:952–60.
[5] Sabelli R, Bruneau M. Design guide 20: steel plate shear walls. Chicago, IL: American Institute of Steel Construction; 2007.
[6] ATC. Guidelines for seismic testing of components of steel structures. Tech. Rep. 24. Applied Technology Council, Redwood City, CA; 1992.
[7] Vian D, Bruneau M, Tsai KC, Lin Y-C. Special perforated steel plate shear walls with reduced beam section anchor beams. I: Experimental investigation. J Struct Eng 2009;135(3):211–20.
[8] Clayton PM. Self-centering steel plate shear walls: subassembly and full-scale testing, general exam. Seattle, WA: Civil and Environmental Engineering Dept., University of Washington; 2012.
[9] Baldvins N, Berman JW, Lowes LN, Janes T. Development of damage prediction models for steel plate shear walls. Earthq Spectra 28 (2).
[10] Li C-H, Tsai K-C, Lin C-H, Chen P-C. Cyclic tests of four two-story narrow steel plate shear walls. Part 2: Experimental results and design implications. Earthq Eng Struct Dyn 2010;39:801–26.
[11] Tromposch EW, Kulak GL. Cyclic and static behaviour of thin panel steel plate shear walls. Structual Engineering Report 145, Dept. of Civil Engineering, University of Alberta, Edmonton, Alberta, Canada; 1987.
[12] Berman JW, Bruneau M. Experimental investigation of light-gauge steel plate shear walls for the seismic retrofit of buildings. Technical report MCEER-03-0001, Multidisciplinary Center for Earthquake Engineering Research, Buffalo, New York; 2003.
[13] Basler K. Strength of plate girders in shear. Fritz Laboratory Report 251-20, Lehigh University, Fritz Laboratory, Bethlehem, Pennsylvania; 1960.
[14] Thorburn LJ, Kulak GL, Montgomery CJ. Analysis of steel plate shear walls. Structual Engineering Report 107, Dept. of Civil Engineering, University of Alberta, Edmonton, Alberta, Canada; 1983.
[15] Xue M, Lu LW. Interaction of infilled steel shear wall panels with surrounding frame members. In: Proceedings of the structural stability research council annual technical session, Bethlehem, PA; 1994. p. 339–54.
[16] Mazzoni S, McKenna F, Scott M, Fenves G. Open system for earthquake engineering simulation user command-language manual – OpenSees version 2.0. Pacific Earthquake Engineering Research Center, University of California, Berkeley, Berkeley, CA; 2009.
[17] Berman JW, Bruneau M. Experimental investigation of light-gauge steel plate shear walls. J Struct Eng 2005;131(2):259–67.
[18] Shishkin JJ, Driver RG, Grodin GY. Analysis of steel plate shear walls using the modified strip model. Structual Engineering Report 261, Dept. of Civil Engineering, University of Alberta, Edmonton, Alberta, Canada; 2005.
[19] Webster D. The behavior of un-stiffened steel plate shear wall web plates and their impact on the vertical boundary elements. Ph.d. dissertation, Civil and Environmental Engineering Dept., University of Washington, Seattle, WA; 2013.